

Study of Two-Phase Microchannel Heat Sink Fabricated by A.M. Technology for Energy Reuse in the Electronic Device

Nan Chen*, Yunshui Chen and He Zhao

Advanced Liquid Cooling Technologies, Greenville, USA

*Corresponding author. E-mail: brad.chen@advancedliquidcooling.com

Abstract

Data centers' electricity energy consumption accounts for 1% of global electricity demand and 0.3% of all global CO₂ emissions. Energy reuse as a core of a net zero carbon data center, as a macro goal benefiting to mankind, needs micro innovations from thermal engineers to reclaim the distributed and low-grade thermal energy from diversified electronic equipment. This article presents the attempt to combine the advantages of high-density heat transferring technology by two-phase microchannels and the agility of Additive Manufacturing (A.M.) technology into a heat sink by which thermal energy can be collected in premium quantity and quality. The heat sink prototype adopted the two-layer microchannel design by leveraging the unique capability of A.M. technology to form complicated spatial geometric features, such as the functional channel profiles with diverged cross-sections along the flow direction, intermittent channels, and curved channels. It was fabricated at one-time processing by AlSi10Mg powder SLS/SLM, had an exterior base area of 25 cm², and interior micro-fins with a minimal thickness of 0.2 mm and fin pitch of 0.38 mm. A test rig had been built to validate the thermal dynamic and hydraulic performance of this microchannel heat exchanger working with HFE 7100 as the coolant. The heat flux under certain wall superheat and pressure drop catches the equivalent grade of microchannels made by conventional micro-cutting approaches on copper or aluminum. The maximum inlet coolant temperature could be elevated up to 60.0 °C with less than 90.0 °C CPU case temperature, which provides the feasibility of high-grade heat recovery. The test results present the promising prospects of this design and A.M. technology in the field of two-phase microchannel heat exchanging, by which the electronic devices in megawatt hyperscale data center can be changed from energy consumers to energy generators for the greenhouse, district heating, and hot water system.

Keywords: heat transferring, two-phase boiling, microchannel, heat sink, additive manufacturing, energy reuse

Citation

Nan Chen, Yunshui Chen and He Zhao (2022), Study of Two-Phase Microchannel Heat Sink Fabricated by A.M. Technology for Energy Reuse in the Electronic Device. *Green Energy and Environmental Technology* 2022(0), 1–19.

DOI

<https://doi.org/10.5772/geet.09>

Copyright

© The Author(s) 2022.

This is an Open Access article distributed under the terms of the Creative Commons Attribution License (<https://creativecommons.org/licenses/by/4.0/>), which permits unrestricted reuse, distribution, and reproduction in any medium, provided the original work is properly cited.

Published

30 August 2022

1. Introduction

According to the International Energy Agency, data centers consume around 200 terawatt-hours (TWh) of electricity, which accounts for 1% of global electricity demand and 0.3% of all global CO₂ emissions [1]. Data center operators and trade associations are committed to the European Green Deal to make data centers climate neutral by 2030 as an integral part of the ambitious goal of making Europe climate neutral by 2050 [2]. Climate neutral data centers will be measured by Net Zero results [3]. The concept of Net Zero data center includes not only the reduction of data center energy consumption by location-based renewable energy, elevating clean energy production and data center energy efficiency, no water use, pollution reduction but also focusing more on the circular energy and economy system, i.e., the reuse of data center heat. District heating, evolving to the 4th generation, has integrated more flexible and clean energy sources into the energy mix for the goal of Net Zero Emission. The share of renewable and electricity energy in global district heat supplies together will rise from 8% to nearly 35% by 2030 and the carbon emission will be cut by more than one-third [4]. The heat from the data center can work as a perfect source for the district heating system.

Although, industry leaders are realizing and urging the role transition of electronic devices from pure energy consumers to energy generators, by reclaiming the heat dissipated from processors [5], the energy reuse rate in electronic devices is largely restricted by the energy quality, i.e., exergy, as the function of temperature and pressure of the fluid. The higher the temperature of the outlet coolant, the easier the energy transmission will be, and higher energy conservation efficiency could be achieved. To elevate the outlet coolant temperature, on one side the electronic engineers must lift the temperature limits of processors further; on the other side, thermal engineers have to reduce the temperature differential between coolant outlet temperature and case temperature of processors. As a main potential application scenario, the 4th generation district heating system based on more sustainable energy resources at the temperature ranging from 60 °C to 70 °C would be the most common deployment of reclaimed heat from the data center [6]. Moreover, regarding the safe water temperature codes of building hot water systems, 60 °C is recommended by ANSI/ASHRAE Standard 188-2018 as a lower limit to mitigate the legionellosis risk [7]. Therefore, 60 °C–70 °C would be the ideal lower temperature limit for the prospective heat reuse technologies, which cannot be delivered by most of the liquid cooling solutions and all air-cooled solutions [8].

Microchannel heat exchanging technologies have been now one of the most active divisions of heat transfer enhancement, with innovative solutions emerging every day to cater to the increasing demands from electronic cooling, by the adoption of different channel geometrical sizes, materials, coolants, and so on. The holistic

comparison studies of heat transferring performance of microchannel heat exchangers [9–11] prove that two-phase flow in microchannels can create lower thermal resistance under the conditions of increasing heat flux and decreasing hydraulic diameter. As supportive evidence, the data in the experimental study [12] indicated more uniform chip temperature gradients, 40.0–80.0 times lower pumping power consumption, and more than 150.0 W/cm² heat flux can be realized. Similar conclusions had been drawn by Karwa [13] that two-phase cooling could achieve lower junction temperatures and more uniform cooling at a much lower flow rate. Although most previous researchers acknowledged that this technical merit of two-phase flow in a singular microchannel implies a brighter technical and eventually commercial future [14, 15], there are many technical barriers to the complete microchannel heat sink to be adopted by the electronic industry, from the special characteristics of two-phase flow thermal performance and manufacturing cost/methods, mostly resulting from the geometrical magnitude of the microchannel, to be overcome.

Some pioneers have attempted to fabricate and investigate the complete two-phase microchannel heat sinks. Recinella [16] designed two microchannel heat exchangers (length 1 cm × width 1 cm, distilled water as working fluid) with radial and diverged cross-sectional area microchannels and offset strip fins, with the intent to attenuate the two-phase boiling instabilities. Testing results of radial microchannels with an added gap present a maximum heat flux of 385.5 W/cm² at 42.7 °C wall superheat 140 kPa pressure drop, while the offset strip fin configuration achieves much higher heat transfer performance with CHF values exceeding 900.0 W/cm² at 58.6 °C walls superheat and 190.0 kPa pressure drop. Song [17] designed three microchannel heat exchangers (Novec 7000 as working fluid) with radial and divergent cross-sectional microchannels. Under the operation conditions of the heating load of 400.0 W and flow rate of 8.0 L/h, the maximum measured wall-temperature, the calculated averaged heat transfer coefficient, and the pressure drop were 104.0 °C, 0.009 kPa, and 65.4 kW/m²·K, respectively. This design intends to mitigate the flow boiling instability by the concepts of diverged and segmented microchannels. Qualitative explanations have been done with reference to the diagram of Ledinegg and the pump curve. As the results of theoretical prediction, the heat exchanger with cutting in its cold plate and without a gap in its cover has the best performance in a two-phase flow cooling system. Its peak heat transfer coefficient could reach about 550.0 kW/m²·K, under the condition of water flow 12.0 L/h and heat load 300.0 W. Regarding the data regression method, the heat flux and relevant thermal parameters were overestimated by their calculation based on the finned area (28.0 cm²) rather than the thermal affected area of the heat sink (125.1 cm²). The corrected max. heat flux of this heat sink is 4.8 W/cm². The proximity of the profile design topology by Recinella [16] and Song [17] is high. The common points in their conclusions are (1) the effects of diverged and segmented

channels on the improvement of thermodynamic and fluid dynamic performance could be observed; (2) high wall superheat is required, which makes them not suitable to cool CPU regarding case temperature upper limits as 80.0 °C in most cases. Joshi [18] tested a two-layer branching microchannel heat sink using HFE-7100 as the coolant. The peak heat transfer coefficient of the heat sink is 28,700.0 W/m²·K at a heat flux value of 174.0 W/cm², a flow rate of 450.0 ml/min, and wall overheat 62.0 K. Under HFE-7100 liquid inlet temperature of 55.0 °C, the case temperature of the heat source would be 117.0 °C, which is above the permitted temperature of most processors. This design has been patented [19–21] by Toyota Research Institute of North America, the potential applications of this design would be battery cooling in E.V. In this article, all thermal-related parameters are calculated based on a 1.9 cm × 1.9 cm finned area rather than the heat sink base area of 7.0 cm × 7.0 cm. The aluminum manifold welded with the finned area can assist in dissipating heat to the internal working fluid. Regarding the 13.6 times area difference between base area and finned area, the corrected peak heat flux would be 12.8 W/cm². Ali's experimental study [22] achieved base heat flux up to 335.3 kW/m² for a hot chip area of 500 mm² at the case temperature of less than 80 °C, and a maximum two-phase heat transfer coefficient of 12.7 kW/m²·K at a mass flux of 250.0 kg/m²·s @ 15.0 K wall superheat by HFE7100 at the parallel straight microchannels. Compared with Joshi's testing data, the heat transfer coefficient in Ali's study (12.7 kW/m²·K @ 15.0 K) is half of Joshi's results (28.7 kW/m²·K @ 62.0 K). Referring to its 15 K wall superheat and 54.6 °C inlet temperature, a wall temperature of 69.6 °C makes it suitable to cool most electronic devices, i.e., CPU and GPU. The peak heat flux 335.3 kW/m² @ 17.0 K is calculated by the chip area as 500 mm². The inlet and outlet plenum area (314.0 mm²) machined as a part of the complete copper heat sink has been ignored, in which heat transferring to working fluid happened indeed. If this area correction is included, the peak heat flux would be reduced from 335.3 kW/m² to 20.6 W/cm². In this testing, flow reversal was observed for all mass fluxes due to the rapid bubble generation near the channel inlet and slug formation, which is hard to be avoided in straight channels.

Subtractive machining micro-deformation, micro sawing, micro-milling, and dicing have been conventionally used in microchannel fabrication [23]. These fabrication approaches suffered from geometric restrictions of specific machining tools. Complex design features such as three-dimensional curves or channels, multilayers, integrated inlet/outlet ports, and internal chambers are extremely difficult or impossible to be fabricated. The machining accuracy and surface quality rely heavily on the design of the cutting tool. The majority of commercial microtools [24] are scaled-down versions of conventional microtool designs, which have the disadvantages of short life by wearing, cracking by mechanical stress, fatigue fracture, and high cost. The accumulated wear and deformation of microtools will deteriorate the clearance alignment between microchannels, and

even between heat sinks. Besides the difficulties in getting suitable and reliable machining tools, the mechanical cutting itself has disadvantages of long fabrication time, risks to cause chipping/fracture of the substrate, and incapability to form the internal chamber. Micro sawing [16–18] is the major method to be used at present, which retains all drawbacks micro-mechanical cutting has. In addition, the curved profile for sawing technology will be a time-consuming task and consequently a poor cost-effective option. Secondary machining is usually required if the selection of sawing steps cannot result in the expected wall smoothness. The compression molding [18–21] is another approach to get the microchannel heat sink. However, regarding the cost of mold development and accuracy of molding processing, it is not an economic and precise, and is an option only when the production volume is massive. For the internal chamber formation inside the heat sink, all previous studies rely on an extra assembled cover on the top of the finned area, which will create more failure modes, like seal leaking, tolerance mismatch, bonding/weld deformation, and so on.

A practical microchannel heat exchanger aiming at extensive commercialization for the thermal energy reclaim must own several critical elements, such as high performance at low wall superheat, manufacturability, cost-effectiveness, and flexibility/adaptability to variable applications. In order to catch the above elements, efforts have been done to design a microchannel heat sink with a curved wall profile, fabricate samples by A.M. technology, and validate their effectiveness by testing.

2. Microchannel heat sink design

The strategy of overfeeding pump refrigerant system [25, 26] has been used to achieve stable and high-efficiency evaporation. Figure 1(a) is a cross-sectional drawing of a microchannel heat sink sample, in which 1st, the 2nd layers, and all components are printed at one time. The liquid from the Liquid in port into the heat sink goes into the Liquid distribution plenum, in which the liquid velocity is reduced due to its volume expansion for even flow distribution between microchannels. Meanwhile, the liquid at its subcooling state impinged from the top to the bottom of the plenum can cool the core of the heat source more effectively. Then liquid with less subcooling will be driven into the channels formed by the micro-fins in Circle one at both 1st and 2nd layers. The rectangular cross-section between micro fins diverges along the direction of length in alignment with the expansion of liquid volume due to the small fraction of bubbles. The curved micro-fins will create more vortices to improve the heat transfer coefficient in the stage of subcooled boiling. The intermittent micro-fins between Circle one and Circle two will not only provide the space for the rebalance and the mixture of liquid and vapor but also destroy the developed boundary layer on the micro-fins at Circle one and make the thickness of the initial boundary on the micro-fins at Circle two thinner than that on the

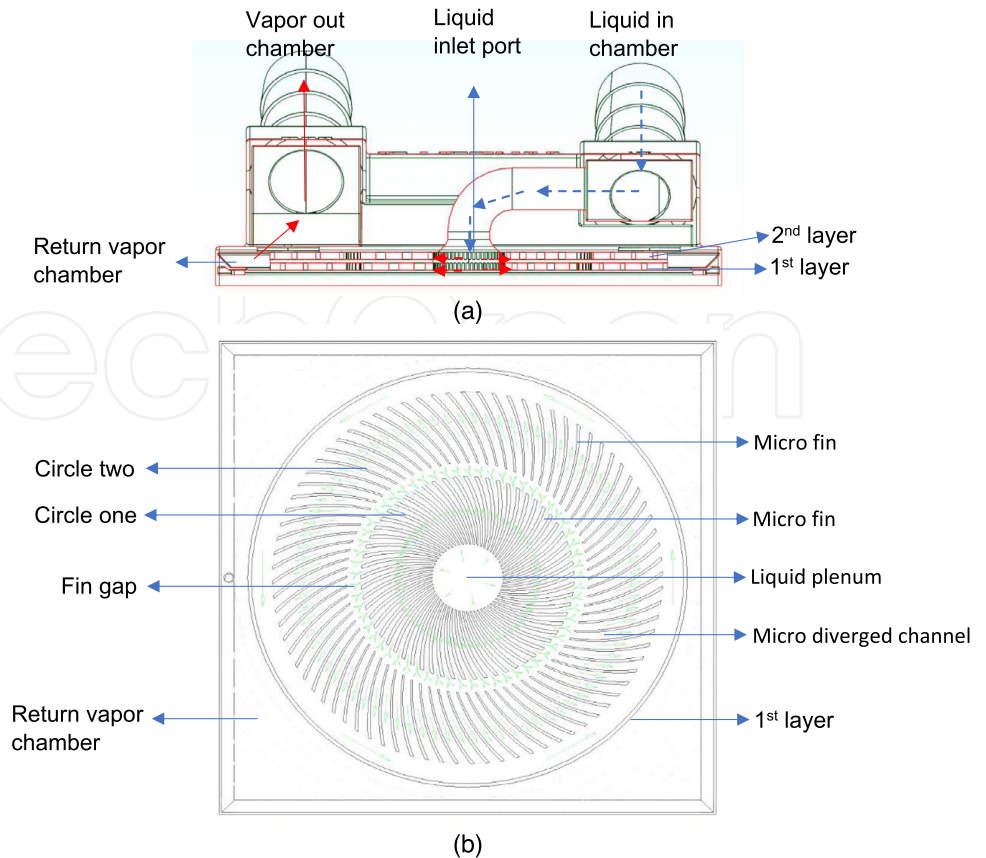


Figure 1. (a) Cross-sectional drawing of microchannel heat sink; (b) schematic diagram of flow in microchannel cold header.

continuous micro-fins. The strong turbulence and vortex by liquid/vapor flushing on the tip of micro-fins at Circle two will booster heat transferring. The same philosophy of channels in Circle two as that in Circle one has been adopted. The larger flow area in Circle two formed by a longer arc length than that in Circle matched the fact that more bubbling is contained downstream of boiling flow. The liquid/vapor mixture out of the channel in Circle two will be collected in the Return vapor chamber, and then flow out of the heat sink from Vapor out chamber.

3. Microchannel heat sink manufacturing

Overall, A.M. technologies can be divided into three main categories based on how the material is formed into the object [27]: (1) Fused filament fabrication (FFF)/fused deposition modeling (FDM); (2) Stereolithography (SLA); (3) Selective laser sintering/melting (SLS/SLM). The first two AM methods (FFF/FDM and SLA) are most suitable to print polymers, ceramic and compound materials making them ideal for printing insulation components in an electrical machine. SLS/SLM printing uses a laser to heat the raw material (metal powder), allowing a

Table 1. Chemical composition of AlSi10Mg, wt%.

Al	Si	Mg	Fe	Ti	Mn	Cu	Ni	O
Bal.	9–11	0.2–0.4	≤0.55	≤0.15	≤0.45	≤0.03	≤0.04	Reported

significantly higher temperature to be achieved. This makes it suitable to print different metals by complex spatial dimensions, which is critical for the fabrication of microchannel heat exchange. Referring to the typical minimum features, sizes of 0.2–0.4 mm with the maximum part size of about 300.0–400.0 mm cover a range suitable for most small/medium part size requirements [28]. Larger systems are now becoming available using multiple laser sources for enhanced productivity and with build volumes up to 500.0 × 280.0 × 850.0 mm. Even larger systems (>1.0 m) are being developed but are not commercially available or widely accessible yet. Collins *et al.* [29] used SLS/SLM in their work to produce both straight and manifold microchannel designs with hydraulic diameters of 500 μm in an aluminum alloy (AlSi10Mg). Thermal and hydraulic performance was characterized over a range of mass fluxes from 500.0 kg/m²·s to 2000.0 kg/m²·s using water as the working fluid. It can be found that the nominal geometries are reproduced accurately enough to predict pressure drop based on conventional hydrodynamic theory albeit with the roughness-induced early transition to turbulence, but the uncertainty of thermal performance is existed due to the unknown properties of printed metal. Jain [30] discussed the unique capabilities of A.M. in the field of thermal management, which are (1) High precision liquid-cooled microchannels can be realized by the features with as small as 20 μm dimension and ±2 μm tolerances; (2) Increased surface area to enhance convection; (3) Integrated composite structure with optimized material pallet. A.M. used to fabricate the microchannel heat exchangers is not a challenge [31, 32], the real challenge is how to design a microchannel heat exchanger which can achieve good performance by virtue of the advantages of A.M., especially in the application of the two-phase boiling.

Aluminum can be used to produce lightweight, geometrically complex parts due to its advantages such as lightweight material with good alloying properties, high corrosion resistance, easy post-processing (e.g., to machine, weld, and polish), high strength-to-weight ratio, high-temperature resistance, and thermal and electrical conductivity. AlSi10Mg is a widely used alloy powder in SLS/SLM, that combines lightweight and good mechanical properties. Specimens were manufactured from gas atomized AlSi10Mg powder of spherical shape with a size distribution between 20 and 63 μm, its composition is shown in Table 1.

The microchannel heat exchanger sample was fabricated by a Laser Powder Bed Fusion machine (LPBF). During specimen production, the O₂ concentration in the LPBF chamber was maintained below 500.0 ppm and the base plate was maintained at 80.0 °C [33]. After-manufacturing heat treatment and stress-relief had been done



Figure 2. Cross-sectional view of microchannels fabricated by A.M.

to achieve good thermal and mechanical performance. It has been proved that T6-like heat treatment can improve both mechanical and thermo-mechanical performance [34]. With different manufacturing angles, the thermal conductivity will vary from 165.0 W/m·K in vertical to 155.0 W/m·K in horizontal. The surface roughness R_a (μm) will vary with the manufacturing angle from 8.0 μm on vertical to 67.0 μm at a 30.0° angle on the horizontal. Acknowledged that surface modification on metal parts has been validated as an effective approach to improve the two-phase boil heat transfer [35], similar effects of the surface roughness on the boiling heat transfer are expected to be achieved on the parts made by A.M. Refer to figures 2(a) and (b), due to the limits of minimal wall thickness (0.2 mm), the thickness of the micro-fin tip at Circle one is 0.20 mm and the corresponding width between two micro-fins is 0.38 mm. The thickness of the micro-fin tip at Circle two is 0.22 mm and the corresponding width between two micro-fins is 0.99 mm. The diameter of the liquid distribution plenum is 10.0 mm and the gap between Circle one and two is 2.0 mm. The thickness of the bottom plate is 2.0 mm at this moment regarding the requirements of deformation control to achieve a certain flatness coupling with heat sources. This design is an optimal option after trying different configurations with the considerations of performance, manufacturing stability, printing speed, heat treatment deformation, and cost.

4. Microchannel heat sink testing rig

A schematic diagram and the experimental facility itself are depicted in figures 3 and 4 respectively. This rig consisted of two main parts: the test loop and an auxiliary cooling loop. The test loop included a liquid reservoir, DC permanent magnet centrifugal pump (with an inverter for step-less speed control flow rate), flow meters, and the microchannel heat sink test section. Silicon Controlled Rectifier (SCR) was used to control the input power to cartridge heaters, imbed in the copper block, then the heat flux for the microchannel heat sink could be adjusted and read

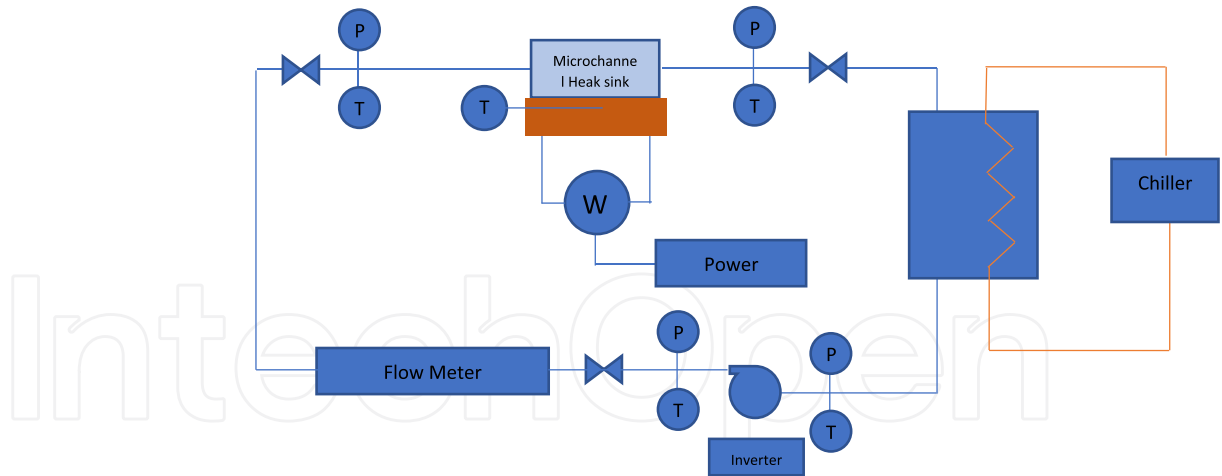


Figure 3. Schematic diagram of the testing rig.



Figure 4. Testing rig of the microchannel heat sink.

through the power meter. The fluid flow rate during the experiments was controlled/adjusted by this high-precision digital driver connected to the centrifugal pump. This pump suctions the liquid from the bottom of the reservoir to make sure there is no cavitation in the suction port. The working fluid HFE 7100 was circulated by the pump, boiled in the microchannel heat sink, and then condensed by the cooled water from the chiller in the reservoir. The spiral 9.5 mm copper tube in the reservoir provides enough condensation area for HFE 7100 vapor, and the liquid level of HFE 7100 was kept in half of the reservoir, in which the reverse flow between cooled water (flow in from the bottom and flow out from the top) can provide subcooled liquid at the bottom outlet port of reservoir. The system pressure is supervised by the pressure probe on the top of the reservoir, by which the saturated temperature and then subcooling temperature can be calculated. Temperature sensors and pressure sensors are installed at the inlet and outlet of the

pump respectively for pumping head and piping pressure drop. The pressure and temperature sensors before and after the microchannel heat sink can obtain the pressure drop on it. The auxiliary cooling loop was a re-circulating chiller system with a cooling capacity of 2.0 kW. Secondary coolant (water) will be circulated through the copper coil in the liquid reservoir to absorb the condensing heat and sub-cool the bottom liquid in the reservoir. The outlet water temperature can be maintained automatically at the setpoint, and cooling capacity could be shown on the screen on the control panel in the chiller by the calculation of mass flow and temperature differential.

All the measuring instruments, pressure transducers, thermocouples, and flow meters, were connected to the data logger. This logger was connected to a computer with logging software to record and save all the measured data after the system reached a steady state. Their specifications are shown in Table 2.

5. Data reduction

The test section utilizes a nickel-chromium resistive element heater (cartridge heater, 10.0 mm × 65.0 mm, 300.0 W, max. temperature 450.0 °C) powered by an SCR power supply. The input power is obtained directly from the power supply through the power meter which is utilized to measure the electrical input parameters of the heater including voltage, current, and power factor. The input heat flux to the heat sink surface is then calculated as the difference between the total power, Q_{tot} , and the predicted test section heat loss, Q_{loss} , over the bounding area of the resistive heater, A_h . Here,

$$q'' = (Q_{tot} - Q_{loss})/A_h, \quad (1)$$

where Q_{loss} is obtained using the heater temperature, T_h measured via the device center thermocouple. The material around the heater is FR4 PCB glass fiber laminates (contacting area = 32.0 cm²), which have a thermal conductivity of 0.25 W/m·K [36]. Rigid polyurethane (PU) flame-retardant foam with its thermal conductivity as low as 0.022 W/m·K to 0.028 W/m·K [37] was used to insulate the bottom of heaters (contacting area = 128.0 cm²).

Based on our experimental results, we estimated that <3.0% of heat generation power was lost through conduction to ambient.

$$Q_{loss} = \left(\frac{k}{s}\right) \times A \times (T_h - T_i) \quad (2)$$

s = material thickness (m), A = heat transfer area (m²), k = thermal conductivity of material (W/m·K), Q_{loss} = heat transfer (W).

Utilizing the input heat flux, q'' in equation (1), the effective heat transfer

Table 2. The specifications of main components.

Datalogger	OHR-H700	Measurement accuracy: 0.2% FS ±1 digit Response time: ≤1 s Temperature drift ≤0.01% FS/°C (typical 50 ppm/°C)
Pump:	OWP- BL43-450T	High-efficiency brushless DC motor PWM signal speed controlling
Cartridge heater		220 V AC @: 300 W ± 10% High-temperature nickel-chromium lead wire up to 450 °C
Power meter	PM9800	Power range: 0.1 W–12 kW; power factor range: 0.001–1.000 Calculation method: watt (W) ÷ [voltage (V) × current (A) = power factor (PF) Frequency range: 40–400 Hz Basic accuracy: ± (0.4% reading + 0.1% range) Measurement speed: 3 times/s
Power supply	RioRand	Maximum power: 4000 W Voltage adjustment range: AC 0–220 V
Chiller	ALH-2000	Cooling capacity: 2000 W (6824 BTU/h) with 25 °C liquid-ambient delta @ 8.8 LPM Heating capacity: 1000 W The temperature in °C/°F with a set-point based on: liquid, or one of two optional K-type thermocouples
Flowmeter	LW- 15Z1AWNSR-TG	DN15, accuracy: ±0.5% @ 8–50 L/min, temperature range –40–120 °C

coefficient, h , can then be determined in equation (2) as a function of the measured heater temperature, T_h , and coolant fluid inlet temperature, T_{in} , as follows:

$$h = \frac{q''}{(T_h - T_{in})} \tag{3}$$

The pressure drop, ΔP , across the test section is measured directly using the differential pressure transducer and is the difference in equation (3) between the inlet pressure, P_{in} , and outlet pressure, P_{out} , of the test section,

$$\Delta P = P_{in} - P_{out} \tag{4}$$

Table 3. Experimental measurement accuracy.

Measured value	Instrument	Error/uncertainty range
Temperature sensors	PT100	± 0.1 °C
Copper heater	RTD	$< 0.04\%$
Pressure probes for HFE 7100	Piezoresistive pressure transducer	$< \pm 1.2\%$
Pressure probes for water	Piezoresistive pressure transducer	$< \pm 2\%$
Mass flow rate	Turbine flow meter	$< \pm 0.5\%$
Power meter		$< \pm 0.5\%$

Table 3 shows the accuracy of individual instruments. As a critical parameter, the heat flux is directly read from the power meter with an error of less than $\pm 0.5\%$. The rest of the parameters read directly from meter and sensors have their original uncertainties as listed. The uncertainties of the heat transfer coefficient are calculated by equation (1) has an uncertainty of 0.7% as the summary of the uncertainty of heat flux and temperature differences. The presentation of the experimental results omits uncertainty bars to improve the visualization of the data.

6. Experimental results

Figure 5 presents variations of CPU temperature and saturated temperature in the liquid reservoir under different volumetric flows and at a constant heat load of 700 W. The saturated temperature of 3M HFE 7100 is calculated as the function of logged pressure in the liquid reservoir by the regression equation from the pressure-enthalpy chart. As a hermetic system, when the external flow rate increases, the internal pressure in the reservoir can be maintained constantly. As a result, the corresponding saturated evaporating temperature in microchannels won't be changed by the fluctuation of the flow rate. However, it can be found that the flow rate can impact the CPU temperature linearly. Increasing the flow rate can clearly reduce the CPU temperature, which indicates an effective approach to avoid overheating the CPU. In the experimental study, when the heat load was reduced from 700 W to 600 W and kept at a constant flow rate of 6 L/min, the pressure in the reservoir drops from 0.43 bar to 0.36 bar this observation indicates that the heat load is the critical factor and has a positive correlation to system pressure will float accordingly, which will impact the boiling parameters such as incipient boiling point, critical heat flux, and so on. Similarly, it could be found that under constant heat flux input of 10.28 W/cm^2 (600 W heat load), the saturated temperature has a minor change of 0.78% with the volumetric flow increasing from 4.34 L/min to 5.58 L/min. In contrast, under the constant volumetric flow of 5.6 L/min, the

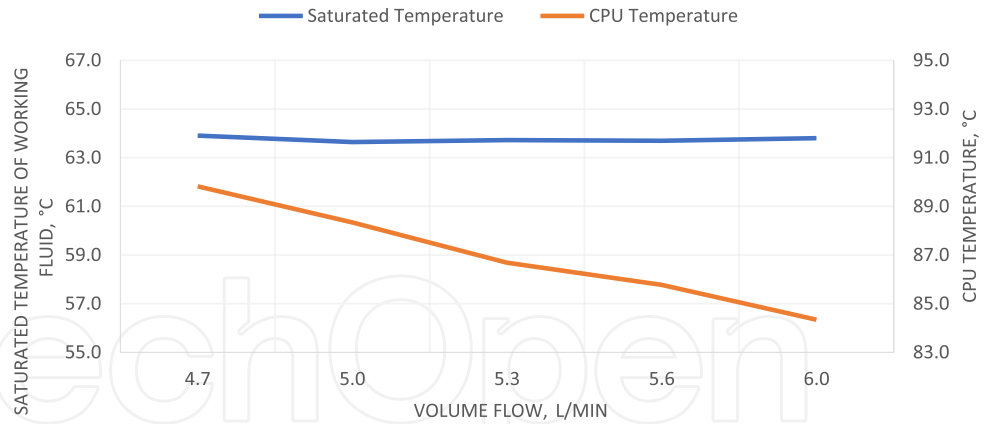


Figure 5. Saturated pressure and CPU temperature variation with volume flow.

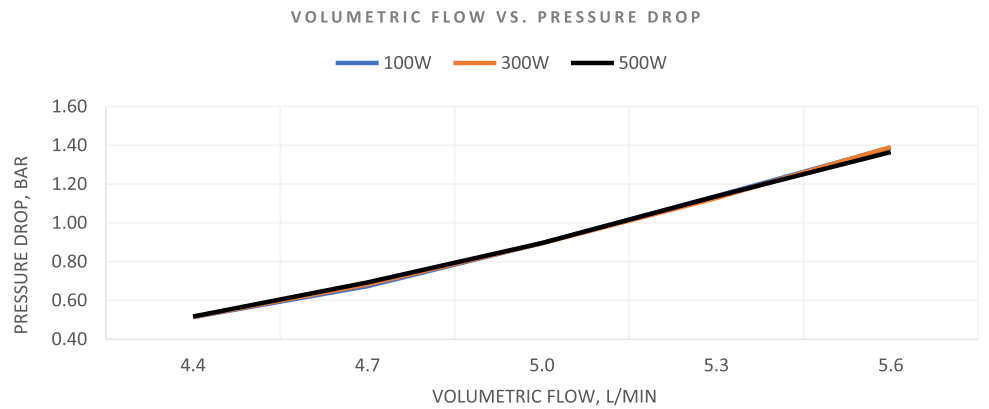


Figure 6. Hydraulic performance of microchannel heat exchanger.

saturated temperature will vary from 63.9 °C to 67.8 °C (6.1%) with the heat flux increasing from 2.1 W/cm² to 10.3 W/cm². In conclusion, the flow rate is the main influential factor in CPU temperature; the heat load is the main influential factor in system pressure. These characteristics will be referred to in the control system design for the optimal CPU operation conditions.

The results of the pressure drop as a function of the input heat flux volumetric flow under different heat loads are presented in figure 6. Experimental results indicate that the pressure drop through the microchannel channel heat exchanger has an almost linear relationship with the volumetric flow regardless of the heat load varying from 100 W to 300 W. During the testing, the inlet subcooling of HFE7100 was maintained constantly at about 15 K, by which the hydraulic characteristic of two-phase fluid at its subcool boiling regime is similar to that of single-phase liquid, due to the limited percentage and strength of bubbling in the flow. It can be predicted that without inlet subcooling, the pressure drop under a higher heat load

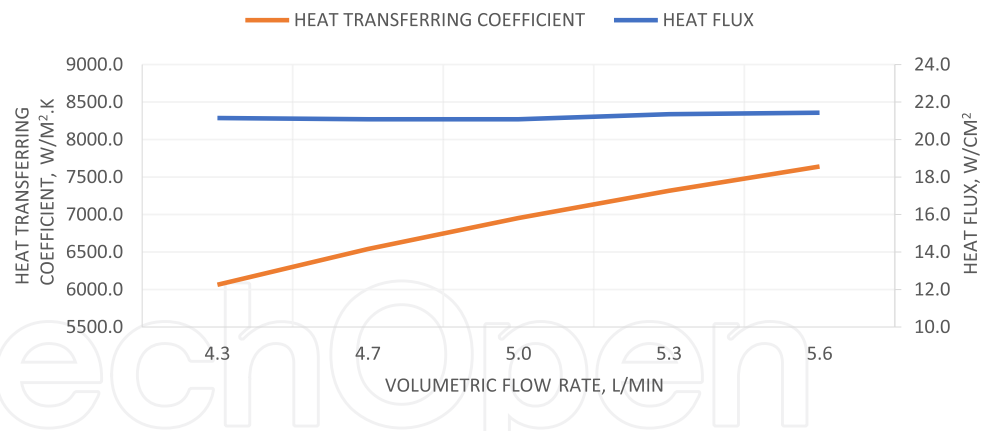


Figure 7. Thermal performance of microchannel heat exchanger.

must be higher than that under a low heat load because of the presence of more bubbles. This characteristic provides a clue to achieving the stable flow of two-phase boiling in microchannels.

Figure 7 is the thermal performance of the microchannel heat exchanger under different volumetric flows. At the point of volumetric flow 5.3 L/min, heat flux 10.4 W/cm² and pressure drop 1.1 bar, the overheating of the copper heater under the microchannel heat sink regarding the inlet liquid temperature is 29.2 K, and the saturated temperature at this moment is 67.5 °C. The thermal resistance between the bottom internal wall of the microchannel heat exchanger and the temperature probe in the copper heater will create a total 3.3 K temperature differential, including 1.2 K on 5.0 mm copper layer, 1.2 K on 0.08 mm thick grease, and 0.9 K on 2.1 mm aluminum layer. Given that 82.1 °C is the reading of the temperature probe in the copper heater, the surface temperature contacting HFE 7100 liquid is 78.8 °C, which is above its saturated temperature. It implies that the boiling has been started locally in the area in contact with the hot metal surface. The flow pattern is at the regime of developed subcooling boiling [38, 39]. This judgment has been validated by the onsite visual observation that there are microbubbles in the outlet transparent flexible tube. The benefits of selecting the regime of developed subcooled boiling as the working regimes are better reliability and comparatively higher heat transfer coefficient driven by lower wall superheating.

Compared with Song's [17] study, its max. wall temperature was 120.0 °C against 34.0 °C boiling point 1 atm of Novec 7000. 86.0 K overheating makes the fluid to be boiled fully along the microchannels and consequently causes flow instability. The maximum heat rejection on the area of 67.9 cm² is 600.0 W, thereof the real heat flux is 8.8 W/cm². The wall temperature higher than 100.0 °C in this study made this design inapplicable for CPU cooling [40]. Joshi's design [18] focuses on the E.V. battery cooling which can tolerate higher wall superheating. Even though the heat transfer has been driven by up to 62.0 K superheat, the heat flux been corrected to

the whole base area is 12.8 W/cm^2 . The equivalent heat flux shown in figure 7 can be achieved by a much lower superheat. Regarding Ali's results [22], the corrected heat flux is 20.6 W/cm^2 , which is at a much higher level than the above reported. Two reasons are (1) Ali's heat sink was made of copper, which has higher heat conductivity than aluminum and 3D printed aluminum; (2) its work regime located at the full evaporating regime gained higher heat transferring efficiency at the expense of flow instability. Mudawar's study [38, 39] reported the testing results of a straight microchannel heat exchanger based on HFE 7100 fluid. The flow regime for indirect refrigeration cooling could range from single liquid forced convection to single vapor forced convection. The recommended region of the highest heat transfer coefficient is the regime from the point of net vapor generation to the start of slug flow. In practice, maximizing the thermal performance is not achievable without sacrificing the superheating control and instability mitigation, which are the critical factors to determine the reliability of electric devices.

In terms of the potential of energy reuse in this study, the outlet water temperature with 600 W heat load and 5.5 L/min HFE7100 flow rate can be kept stably at $52.8 \text{ }^\circ\text{C}$, which is close to $60 \text{ }^\circ\text{C}$ – $70 \text{ }^\circ\text{C}$ as the ideal temperature range for 4th generation district heating $60.0 \text{ }^\circ\text{C}$ outlet water temperature can be obtained at 700 W heat load and $90 \text{ }^\circ\text{C}$ processor temperature. The improvement opportunities to elevate the temperature further are (1) developing a two-phase fluid with higher saturated temperature; (2) improving heat transferring in microchannel further; (3) improving the thermal conductivity of metal fabricated by A.M; (4) define the best working regime of two-phase fluid in the microchannel heat exchanger. Although, there is still a long way to go, the electronic device with $60.0 \text{ }^\circ\text{C}$ hot water output can supersede the heat pump as the primary heat source or work as the preheating stage for the booster boiler.

7. Conclusions

The idea to reclaim the heat generated by the data center for district heating will eliminate the environmental stresses for both industries. This study explores a technical solution bridging these two scenarios by extracting higher-grade energy from the data center. Max. $60.0 \text{ }^\circ\text{C}$ outlet temperature makes it qualified for the sustainable heat resources of 4th general district heating. In addition, the indisputable agility of A.M. technologies can alleviate the barriers of manufacturability and cost for the extensive deployment of microchannel heat sink. Test results have proved the feasibility of this 3D printed microchannel heat sink sample to collect and transfer max. thermal energy 700 W from heat resources to the secondary coolant at the temperature of $60.0 \text{ }^\circ\text{C}$ under the limits of max. $90.0 \text{ }^\circ\text{C}$ processor case temperature. Due to the adoption of the geometric features of diverged, intermittent, and curved channel profiles, the linear trend of the flow

rate-pressure drop curve and flow rate-heat flux curve presents excellent self-adaptive control characteristics for two phases of boiling instead of the complex thermodynamic and hydronic instabilities of the previous microchannel heat exchangers, which are critical to a singular or multiple heat sink systems in avoidance of flow and thermal hunting. In addition, the details of A.M. manufacturing processes, materials, and heat treatment have been summarized for this sample, which presents unparalleled advantages over the conventional machining methods. Moreover, it is suitable for the diversity of electronic devices. Computer servers in the data center consumed 1% of global electricity. If this portion of energy can be reused, 4.5% carbon emission reduction can be achieved by the district heating industry. This exploration presents the undeniable benefits of global environmental protection.

Data availability statement

The data presented in this study are available on request from the corresponding author.

Conflict of interest

The authors declare no conflict of interest.

Nomenclature

<i>A</i>	area, m ²
<i>h</i>	heat transfer coefficient, W/m ² ·K
<i>k</i>	thermal conductivity, W/m·K
<i>P</i>	pressure, Pa
<i>q</i>	heat flux, W/m ²
<i>Q</i>	heating power, W
<i>s</i>	thickness, m
<i>T</i>	temperature, K

Greek symbols

Δ	differential
----------	--------------

Subscripts

<i>hi</i>	heating ambient
<i>in</i>	inlet
<i>loss</i>	loss
<i>out</i>	outlet
<i>tot</i>	total

References

- 1 IEA [Internet]. Data Centres and Data Transmission Networks - analysis; 2021 [cited 2022 Aug 29]. Available from: <https://www.iea.org/reports/data-centres-and-data-transmission-networks>.
- 2 Climate Neutral Data Centre Pact [Internet]. Self-regulatory initiative; 2020 [cited 2022 Aug 29]. Available from: <https://www.climateutraldatacentre.net/self-regulatory-initiative/>.
- 3 Net Zero Data Centre [Internet]. Net zero data center; 2020 [cited 2022 Aug 29]. Available from: <https://www.netzerodc.com/>.
- 4 IEA [Internet]. District heating analysis; 2021 [cited 2022 Aug 29]. Available from: <https://www.iea.org/reports/district-heating>.
- 5 Sovacool BK, Monyei CG, Upham P. Making the internet globally sustainable: technical and policy options for improved energy management, governance and community acceptance of Nordic datacenters. *Renew Sustain Energy Rev.* 2022;154: 111793, doi: 10.1016/j.rser.2021.111793.
- 6 4DH [Internet]. Home; 2022 [cited 2022 Aug 29]. Available from: <https://www.4dh.eu/about-4dh>.
- 7 Van Kenhove E, Dinne K, Janssens A, Laverge J. Overview and comparison of Legionella regulations worldwide. *Am J Infect Control.* 2019;47(8):968–978. doi: 10.1016/j.ajic.2018.10.006.
- 8 Hantsch A, Weisemann A, Banzer LM, Struckmeier J, Wächter C. Cloud & Heat [Internet]. Pushing the boundary conditions of data centers facilitates innovative circular economy approaches; 2021 [cited 2022 Aug 29]. Available from: <https://www.cloudandheat.com/pushing-the-boundary-conditions-of-data-centers-facilitates-innovative-circular-economy/>.
- 9 Agostini B, Fabbri M, Park JE, Wojtan L, Thome JR, Michel B. State of the art of high heat flux cooling technologies. *Heat Transfer Eng.* 2007;28(4):258–281. doi: 10.1080/01457630601117799.
- 10 Riofrío MC, Caney N, Gruss JA. State of the art of efficient pumped two-phase flow cooling technologies. *Appl Therm Eng.* 2016;104: 333–343. doi: 10.1016/j.applthermaleng.2016.05.061.
- 11 Lu S, Vafai K. A comparative analysis of innovative microchannel heat sinks for electronic cooling. *Int Commun Heat Mass Transfer.* 2016;76: 271–284. doi: 10.1016/j.icheatmasstransfer.2016.04.024.
- 12 Szczukiewicz S, Borhani N, Thome JR. Two-phase flow operational maps for multi-microchannel evaporators. *Int J Heat Fluid Flow.* 2013;42: 176–189. doi: 10.1016/j.ijheatfluidflow.2013.03.006.
- 13 Karwa N, Motta SY. Low-pressure heat transfer fluids for pumped two-phase cooling. In: *2021 20th IEEE Intersociety Conference on Thermal and Thermomechanical Phenomena in Electronic Systems (iTherm)*. IEEE; 2021 Jun. 1. p. 188–196. doi: 10.1109/ITherm51669.2021.9503137.
- 14 Jackson M. Electronics Cooling [Internet]. Reasons to Use Two-Phase Refrigerant Cooling; 2011 [cited 2022 Aug 29]. Available from: <https://www.electronics-cooling.com/2011/03/reasons-to-use-two-phase-refrigerant-cooling/>.
- 15 Galvis E. Single-phase and boiling flow in microchannels with high heat flux [thesis]. University of Waterloo; 2012 Dec.
- 16 Recinella A. Enhanced flow boiling heat transfer in radial microchannel and offset strip fin geometries [thesis]. Rochester Institute of Technology; 2016.
- 17 Mengjie S, Chaobin D, Eiji H. Experimental investigation on the heat transfer characteristics of novel rectangle radial microchannel heat exchangers in two-phase flow cooling system for data centers. *J Therm Anal Calorim.* 2020;141(1):199–211. doi: 10.1007/s10973-019-09090-y.
- 18 Joshi SN, Lohan DJ, Dede EM. Two-phase performance of a hybrid jet plus multipass microchannel heat sink. *J Therm Sci Eng Appl.* 2020;12(1):4044347, doi: 10.1115/1.4044347.

- 19 Fukuoka Y, Dede E, Miyagi K. Toyota Motor Engineering, Manufacturing North America Inc. Electronic assemblies having a cooling chip layer with fluid channels and through substrate vias [patent]. United States patent US 10,192,814; 2019.
- 20 Dede EM, Liu Y. Toyota Motor Engineering, Manufacturing North America Inc. Cold plate assemblies and power electronics modules [patent]. United States patent US 8,427,832; 2013.
- 21 Fukuoka Y, Dede E. Toyota Motor Engineering, Manufacturing North America Inc. Electronic assemblies having a cooling chip layer with impingement channels and through substrate vias [patent]. United States patent US 10,566,265; 2020.
- 22 Al-Zaidi AH, Mahmoud MM, Karayiannis TG. Flow boiling of HFE-7100 in microchannels: experimental study and comparison with correlations. *Int J Heat Mass Transfer*. 2019 Sep 1;140: 100–128. doi: 10.1016/j.ijheatmasstransfer.2019.05.0HG95.
- 23 Kumar AU, Javed A, Dubey SK. Material selection for microchannel heatsink: conjugate heat transfer simulation. In: *IOP Conference Series: Materials Science and Engineering*. vol. 346, (1):IOP Publishing; 2018. 012024 p.
- 24 Boswell B, Islam MN, Davies IJ. A review of micro-mechanical cutting. *Int J Adv Manuf Technol*. 2018 Jan;94(1):789–806. doi: 10.1007/s00170-017-0912-y.
- 25 Bortolin S, Rossato M, Bernardinello S, Del Col D. Investigation of evaporator performance with and without liquid overfeeding. In: *16th International Refrigeration and Air Conditioning Conference*. 2016 Jul Paper 1703.
- 26 Jekel TB, Reindl DT. Liquid refrigerant pumping in industrial refrigeration systems. *ASHRAE J*. 2011 Aug 1;53(8):36–42.
- 27 Ghahfarokhi PS, Podgornovs A, Kallaste A, Cardoso AJ, Belahcen A, Vaimann T, Tiismus H, Asad B. Opportunities and challenges of utilizing additive manufacturing approaches in thermal management of electrical machines. *IEEE Access*. 2021;26(9):36368–36381. doi: 10.1109/ACCESS.2021.3062618.
- 28 Prakash S, Kumar S. Fabrication of microchannels: a review. *J Eng Manuf*. 2015;229(8):1273–1288. doi: 10.1177/0954405414535581.
- 29 Collins IL, Weibel JA, Pan L, Garimella SV. Evaluation of additively manufactured microchannel heat sinks. *IEEE Trans Compon Packaging Manuf Technol*. 2018 Aug 23;9(3):446–457. doi: 10.1109/TCPMT.2018.2866972.
- 30 Jain A, Cohen A. Microfabrica [Internet]. Ultra-Precision Metal Additive Manufacturing for Thermal Management of Microelectronics; 2022 [cited 2022 Aug 29]. Available from <https://www.microfabrica.com/downloads/ultra-precision-metal-additive-manufacturing-for-thermal-management-of-microelectronics.pdf>.
- 31 Collins IL, Weibel JA, Pan L, Garimella SV. Experimental characterization of a microchannel heat sink made by additive manufacturing. In: *2018 17th IEEE Intersociety Conference on Thermal and Thermomechanical Phenomena in Electronic Systems (ITherm)*. vol. 29, IEEE; 2018. p. 171–177. doi: 10.1109/ITHERM.2018.8419588.
- 32 Ozguc S, Pan L, Weibel JA. Optimization of permeable membrane microchannel heat sinks for additive manufacturing. *Appl Therm Eng*. 2021;198: 117490. doi: 10.1016/j.applthermaleng.2021.117490.
- 33 Sandvik [Internet]. Osprey AISi10MG powder for additive manufacturing - data sheet; 2022 [cited 2022 Aug 29]. Available from <https://www.metalpowder.sandvik/4aa26f/siteassets/metal-powder/datasheets/osprey-alsi10mg-and-alsi7mg.pdf>.
- 34 Sélo RR, Catchpole-Smith S, Maskery I, Ashcroft I, Tuck C. On the thermal conductivity of AISi10Mg and lattice structures made by laser powder bed fusion. *Addit Manuf*. 2020 Aug 1;34: 101214. doi: 10.1016/j.addma.2020.101214.

- 35 Jafari D, Wits WW. The utilization of selective laser melting technology on heat transfer devices for thermal energy conversion applications: a review. *Renew Sustain Energy Rev.* 2018;**91**: 420–442. doi: 10.1016/j.rser.2018.03.109.
- 36 Sivabalan M. TI [Internet]. Thermal Comparison of FR-4 and Insulated Metal Substrate PCB for GaN Inverter, Texas Instruments, Application Report TIDA030–June 2019; 2019 [cited 2022 Aug 29]. Available from <https://www.ti.com/lit/an/tida030.pdf>.
- 37 ANPE - Associazione Nazionale Poliuretano Espanso rigido [Internet]. Polyurethane Performance-Thermal conductivity; 2022[cited 2022 Aug 29]. Available from: https://www.poliuretano.it/EN/thermal_conductivity_polyurethane.html.
- 38 Mudawar I. Two-phase microchannel heat sinks: theory, applications, and limitations. *J Electron Packag.* 2011 Dec;**133**(4):041002, doi: 10.1115/1.4005300.
- 39 Lee J, Mudawar I. Low-temperature two-phase microchannel cooling for high-heat-flux thermal management of defence electronics. *IEEE Trans Compon Packaging Manuf Technol.* 2009;**32**(2):453–465. doi: 10.1109/TCAPT.2008.2005783.
- 40 Intel [Internet]. Intel Xeon Processor Scalable Family - Thermal Mechanical Specifications and Design Guide; 2019[cited 2022 Aug 29]. Available from <https://www.intel.com/content/dam/www/public/us/en/documents/guides/xeon-scalable-thermal-guide.pdf>.

IntechOpen

Journal : GEET

Article ID : GEET2022009

AUTHOR QUERY FORM

Dear Author,

While preparing the proofs of your article some questions have arisen. They are listed in the table below.

Please check your proofs carefully and mark your corrections in the margin of the proof. Please also answer all questions in this form and return them together with your marked proof.

No author queries

IntechOpen